The Changing Energy Balance of the Polar Regions in a Warmer Climate

LENNART BENGTSSON

Natural Environment Research Council National Centre for Earth Observation, University of Reading, Whiteknights, Reading, United Kingdom, and International Space Science Institute, Bern, Switzerland

KEVIN I. HODGES

Natural Environment Research Council National Centre for Earth Observation, University of Reading, Whiteknights, Reading, United Kingdom

SYMEON KOUMOUTSARIS

International Space Science Institute, Bern, Switzerland

MATTHIAS ZAHN

Natural Environment Research Council National Centre for Earth Observation, University of Reading, Whiteknights, Reading, United Kingdom

PAUL BERRISFORD

National Centre for Atmospheric Science—Climate and European Centre for Medium-Range Forecasts, Shinfield Park, Reading, United Kingdom

(Manuscript received 18 April 2012, in final form 14 November 2012)

ABSTRACT

Energy fluxes for polar regions are examined for two 30-yr periods, representing the end of the twentieth and twenty-first centuries, using data from high-resolution simulations with the ECHAM5 climate model. The net radiation to space for the present climate agrees well with data from the Clouds and the Earth's Radiant Energy System (CERES) over the northern polar region but shows an underestimation in planetary albedo for the southern polar region. This suggests there are systematic errors in the atmospheric circulation or in the net surface energy fluxes in the southern polar region. The simulation of the future climate is based on the Intergovernmental Panel on Climate Change (IPCC) A1B scenario. The total energy transport is broadly the same for the two 30-yr periods, but there is an increase in the moist energy transport on the order of 6 W m^{-2} and a corresponding reduction in the dry static energy. For the southern polar region the proportion of moist energy transport is larger and the dry static energy correspondingly smaller for both periods.

The results suggest a possible mechanism for the warming of the Arctic that is discussed. Changes between the twentieth and twenty-first centuries in the northern polar region show the net ocean surface radiation flux in summer increases ~18 W m^{-2} (24%). For the southern polar region the response is different as there is a decrease in surface solar radiation. It is suggested that this is caused by changes in cloudiness associated with the poleward migration of the storm tracks.

1. Introduction

The warming of Earth's surface and the lower troposphere during the second half of the twentieth century in the Arctic has been considerable. The increase in the annual average surface temperature for the region poleward of 60°N has been between 1.5 and 2.5 K (Fig. 1a). The impact of this warming has been extensive, including a massive reduction in the Arctic summer sea ice and melting of permafrost in many areas. On the other hand the warming in the Antarctic region has been minor and with the exception of the Antarctic Peninsula, less than 0.5°C (Fig. 1b).

Corresponding author address: Lennart Bengtsson, NERC Centre for Earth Observation, University of Reading, Whiteknights, P.O. Box 238, Reading RG6 6AL, United Kingdom.
E-mail: lennart.bengtsson@zmaw.de

DOI: 10.1175/JCLI-D-12-00233.1

© 2013 American Meteorological Society

Brought to you by MAX-PLANCK-INSTITUTE FOR METEOROLOGY | Unauthenticated | Downloaded 04/11/23 01:41 PM UTC

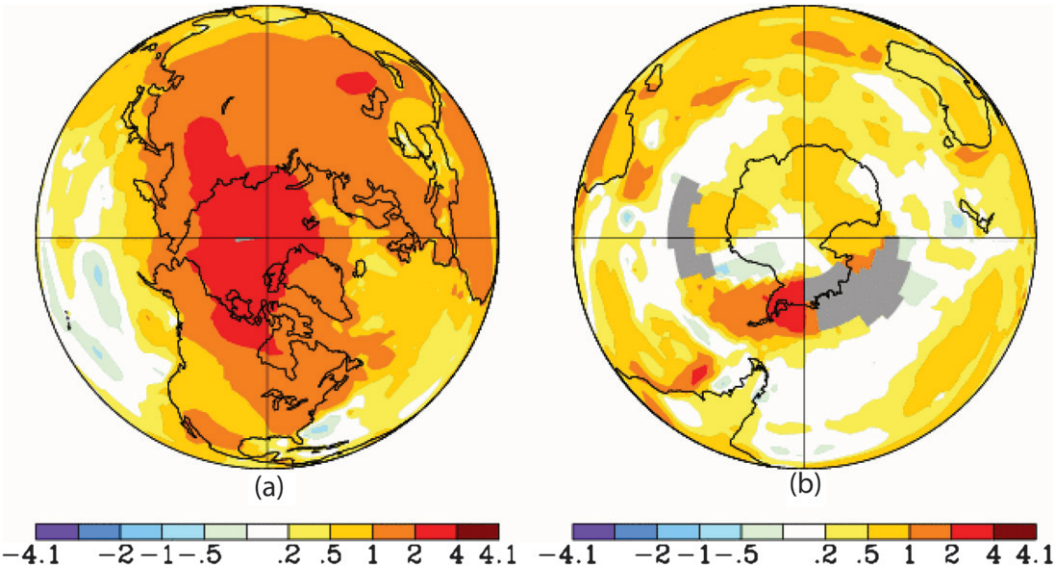

FIG. 1. Trends in surface temperature from the National Aeronautics and Space Administration (NASA) Goddard Institute for Space Studies (GISS) surface temperature analysis for the period 1960–2010: (a) NH and (b) SH. Units are °C (50 yr)$^{-1}$.

The energy transport into high latitudes has been investigated in numerous previous studies, including Budyko (1963), Fletcher (1965), Oort and Peixéto (1974), and Nakamura and Oort (1988), with results summarized in Nakamura and Oort (1988). These early studies were to a large degree based on limited observational records and only the most recent of these had access to independent satellite observations. More recent studies, including Serreze et al. (2007) and Porter et al. (2010) have made use of more advanced space-based observations and reanalyses. However, to obtain meaningful results atmospheric energy transports from the reanalyses must be corrected for mass imbalances. As reported by Porter et al. (2010), the current correction techniques have shortcomings in high latitudes. For this reason they calculated the net horizontal energy transport into the polar regions as a residual using the Clouds and the Earth's Radiant Energy System (CERES) top-of-atmosphere radiation data and an estimate of the net surface flux and the time change in atmospheric energy storage from the reanalyses. As pointed out, this approach has its own shortcomings as the other energy fluxes also have deficiencies, in particular the net surface flux. Recent papers using later versions of reanalyses by Mayer and Haimberger (2012) and by Cullather and Bosilovich (2012) have overcome some of these problems. However, some of the global empirical corrections might influence the regional annual cycle in an unphysical way. We therefore believe that some further development work will be required before reanalyses can be used to estimate the regional energy cycle.

To compensate for the large net radiation to space at high latitudes, large amounts of energy must be transported into the polar regions from lower latitudes. The dominant part of this energy, some 80–85 W m^{-2}, is transported by atmospheric processes. This occurs both in the form of moist energy (latent heat) and dry static energy. The residual part, 10–15 W m^{-2}, enters the polar region through the ocean pathway. The total energy of 90–100 W m^{-2} leaves the atmosphere of the polar regions, as the net difference between the longwave radiation to space and the net incoming shortwave radiation (Nakamura and Oort 1988). The annual cycle of the energy transport has a large amplitude. In late autumn and winter the energy loss due to radiation in the Northern Polar Region (NPR) and Southern Polar Region (SPR) is between 160 and 180 W m^{-2} but in June and July for the NPR and in December and January for the SPR there is in fact a positive radiation balance (gain in energy of the atmospheric column) at the top of the atmosphere, as the net solar radiation is larger than the outgoing net longwave radiation. The surplus of energy is mainly accumulated in the oceans.

As our primary objective is to explore changes in the energy cycle between the present and a future warmer climate we have here used high-resolution simulations with the European Centre/Hamburg Atmospheric Model version 5 (ECHAM5) climate model (Roeckner et al.

Brought to you by MAX-PLANCK-INSTITUTE FOR METEOROLOGY | Unauthenticated | Downloaded 04/11/23 01:41 PM UTC

2003). Relatively high resolution is required since we believe it is essential to be able to resolve intense weather systems as well as different orographic obstacles and complex land–sea contrasts that affects the transport. However, we also contrast the results with those from the lower resolution fully coupled model to check that there are no energetic inconsistencies with the higher-resolution model which is run in a time slice configuration.

A related previous study was recently completed (Bengtsson et al. 2011a) that considered the atmospheric water cycle using data from the same model. It was found, in agreement with Held and Soden (2006), that the transport of water vapor into the polar regions (taken as poleward of 60°N and S) in a warmer climate increases in broad agreement with the Clausius–Clapeyron relation. In the present study we wish to specifically investigate whether there will also be a corresponding reduction of the dry static energy ($c_pT + gZ$) as also suggested by Held and Soden (2006). Such results have also been indicated by Hwang and Frierson (2010) and by Hwang et al. (2011). In the study of Hwang and Frierson (2010) they also found an increasing poleward energy transport with global warming but found also large differences between the different models used in the Intergovernmental Panel on Climate Change (IPCC) Assessment Report 4 (AR4).

The ECHAM5 used for this study has been shown to perform well for various aspects of the general circulation (Reichler and Kim 2008), including weather systems such as tropical and extratropical cyclones (Bengtsson et al. 2007a, 2006, 2009). However, the use of a single climate model will imply a certain restriction on any interpretations of the results that must be kept in mind. A secondary objective of the paper is to explore how the possible changes in the energy transport into the polar regions can help explain the strong warming of the polar regions, in particular the NPR in recent decades.

The paper is organized as follows. In section 2 the data and the methods used to produce the results are discussed; in section 3 the energy processes of the polar regions of the present climate are discussed; in section 4 the polar energy fluxes for the warmer climate are discussed. Finally in section 5 we will summarize the results and suggest further work.

2. Data and analysis methods

The main data used in this study are derived from simulations with the ECHAM5 (Roeckner et al. 2003) atmosphere-only general circulation model (GCM). This is a spectral model and has been integrated at a spectral resolution of T213 (~63 km) using the time slice approach where the lower boundary conditions are supplied from a lower resolution (T63) simulation of the coupled model, ECHAM5/OM, for the A1B scenario produced for the IPCC AR4. The time slice simulations use the same configuration of well-mixed greenhouse gases, stratospheric and tropospheric ozone as used in the lower-resolution coupled model simulations with the lower-boundary conditions of sea surface temperature (SST) and sea ice interpolated from the lower-resolution coupled simulation. Further details of the coupled and time slice simulations can be found in Bengtsson et al. (2006, 2007b), respectively. The time slice simulations cover the two periods 1959–90 and 2069–2100, hereafter referred to as 20C and 21C, respectively. These simulations have previously been used in studies of changes in tropical (Bengtsson et al. 2007b) and extratropical cyclones (Bengtsson et al. 2009) and the transport of water vapor into the polar regions (Bengtsson et al. 2011a) as well as tropical moisture transports (Zahn and Allan 2011, 2013). The results from the Bengtsson et al. (2011a) study are also used here to provide the moist transport part of the energy budget. Comparison of the moisture transport results for 20C with the European Centre for Medium-Range Weather Forecasts (ECMWF) Interim Re-Analysis (ERA-Interim) have shown a broad agreement (Bengtsson et al. 2011a) including the moisture transports in the tropics (Zahn and Allan 2013). We will not discuss this further here as an in-depth assessment of the ERA-Interim energy budget results will be presented in a later study.

Although the objective of this study is to undertake the calculations with the highest possible horizontal resolution consistent with our previous study (Bengtsson et al. 2011a), it may be the case that the lack of coupling to the ocean would introduce problems into the energetic calculation. To check that inconsistencies are not introduced by using the time slice approach the calculations are also performed using data from the original coupled T63 simulation and are compared with those from the higher-resolution time slice simulation. As we show in the appendix, there are only minor differences between the results from the low- and high-resolution datasets and no indication that the high-resolution time slice integration is compromised because of the potential concern of incomplete energy conservation.

The full energy budget of an atmospheric column in terms of the time rate of change of energy (dE/dt) consists of a combination of quantities, which following Nakamura and Oort (1988) can be written as the sum of the net radiation at the top of the atmosphere (F_{RAD}), the vertically integrated horizontal energy flux convergence (F_{WALL}), and the net surface heat flux (F_{SFC}). The top-of-atmosphere radiation is defined as the difference between the top-of-atmosphere net shortwave (F_{SW})

Brought to you by MAX-PLANCK-INSTITUTE FOR METEOROLOGY | Unauthenticated | Downloaded 04/11/23 01:41 PM UTC

and net longwave (F_{LW}) radiation. The net surface heat flux is defined as the sum of the net surface shortwave (SW_{SFC}) and longwave (LW_{SFC}) and the turbulent sensible heat (Q_H) and latent heat fluxes (Q_L).

The horizontal energy flux convergence is formulated as

$$F_{WALL} = \nabla \cdot \frac{1}{g} \int_{p_s}^{0} (c_p T + gZ + Lq + k)\mathbf{V}\, dp.$$

Here, the kinetic energy k is typically ignored as a small contribution (Nakamura and Oort (1988). The other terms consist of the dry static energy $c_p T + gZ$, where c_p is the specific heat capacity at constant pressure, T is the temperature, Z is the geopotential height, and g is the acceleration due to gravity, Lq is the moist energy with L the latent heat of evaporation and q the specific humidity, and $\mathbf{V}$ is the horizontal wind vector. To compute the budget for the NPR and SPR regions the various terms need to be area averaged over these regions. This provides the opportunity to rewrite the horizontal energy transports into the region in a similar way to the study of Bengtsson et al. (2011a) by making use of the Gauss divergence theorem, so that the mean energy transport into the region becomes

$$\overline{F}_{WALL} = \frac{1}{gA} \oint_C \int_{p_s}^{0} (c_p T + gZ + Lq + k) V_n\, dp\, dl,$$

where A is the area of the region, C is the boundary of the region, and V_n is the velocity normal to the boundary (positive inwards). For the simple domains of the NPR and SPR the normal velocity is just the meridional wind with the correct sign. The main reason for taking this approach is that as part of the calculation the transports can be decomposed as a function of location on the boundary, that is, longitude, this then allows us to see where the main transports occur. It is also possible to determine the vertical profiles of the transports by omitting the vertical integration.

The majority of previous studies have calculated the energy transports across 70°N and 70°S. This approach results in several kinds of difficulties in the calculation. First, at these latitudes there are considerable orographic obstacles, making the numerical calculation challenging. Second, a considerable part of the energy transport takes place in the lower part of the troposphere making it necessary to undertake the calculation in model coordinates (Trenberth et al. 2001). Third, energy transports occur in connection with intense transient extratropical cyclones that require a high horizontal and vertical resolution to be realistically simulated. In this study therefore we have performed the calculations of the energy transport at a high resolution in time (6 h) and space (~60 km). The calculations have been carried out in model coordinates following the surface of Earth using the same methodology that was used in Bengtsson et al. (2011a). The reader is referred to this paper for more detailed information on the numerical procedures. This approach is considered essential to obtain reliable results. Finally, we have calculated the transport across 60°N and 60°S to obtain a more representative region and to avoid the problem with the lateral boundary that at 70°N and 70°S cuts through Greenland and a large part of the Antarctic continent respectively.

All other terms in the energy budget are also computed from the 6-hourly data. Finally the 6-hourly data is averaged into monthly, seasonal, and yearly quantities. As with previous studies we use the convention that positive values of the individual terms or their summation indicate an increase in the atmospheric energy content and negative values a decrease.

3. Polar energy fluxes in the present climate

We first summarize the results from the 20C integration and wherever possible compare with results from the space-based radiation data in the form of monthly data from the Energy Balanced and Filled (EBAF) CERES data (Wielicki et al. 1996). In the previous study Bengtsson et al. (2011a) where we investigated the water cycle using the same model it was found that the model depicts the large-scale atmospheric water cycle quite realistically in the polar regions and presumably this is also true for the transport of the dry static energy. A visual display of the annual cycle for various components of the energy budget of the 20C model integration is shown in Fig. 2, for the NPR and SPR, respectively, and the numerical values are given in Table 1 together with the 95% confidence intervals calculated from the standard error of the interannual variability. The different terms are discussed in turn. The rate of change of energy dE/dt is calculated as a residual and as can be seen from Table 1 has a small mean negative bias.

a. The NPR

For the NPR the dry static energy is more than 3 times as large as the moist energy, and the seasonal variation of the two regions also differs significantly (Fig. 2a). The dry static energy has a pronounced peak in winter of more than 100 W m^{-2} but is significantly smaller in summer with only some 25% of the winter transport. The moist transport varies less and peaks in the late summer to early autumn. Both the dry static and moist transports are strictly positive for all individual months.

Brought to you by MAX-PLANCK-INSTITUTE FOR METEOROLOGY | Unauthenticated | Downloaded 04/11/23 01:41 PM UTC

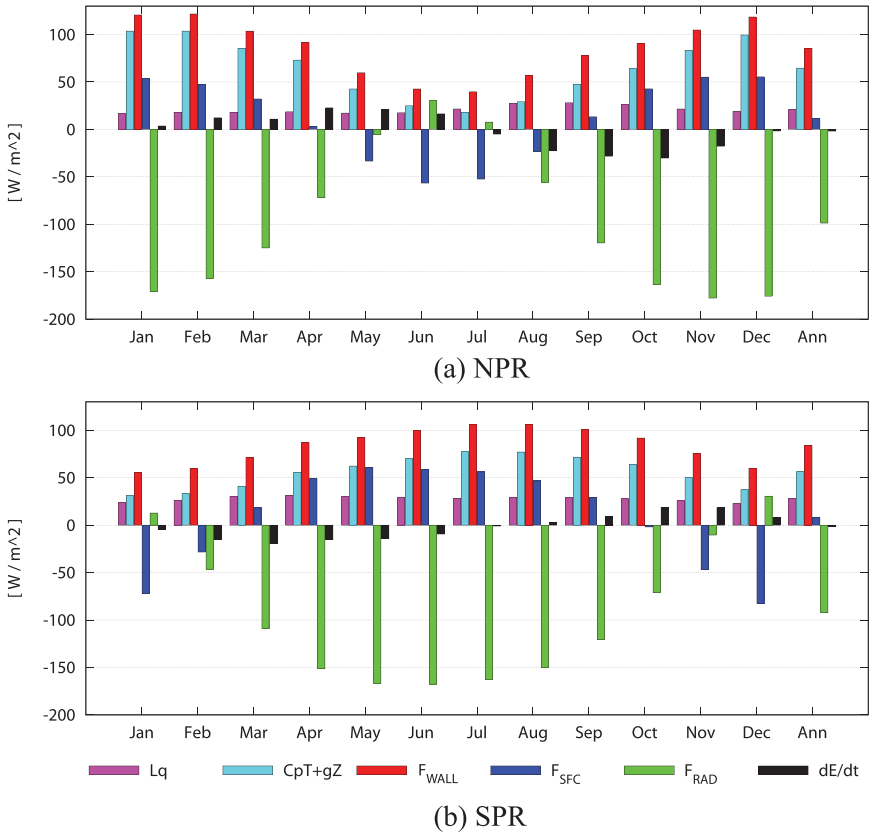

FIG. 2. Annual cycle of components of the energy budget in the (a) NPR and (b) SPR for the model 20C period. Units are W m^{-2}.

The surface fluxes F_{SFC} (top part of Table 1; Fig. 2a) are positive in winter resulting in a positive contribution to the atmospheric energy and a negative contribution in summer. Examining this in more detail the annual cycle has a large amplitude for both ocean and land areas as can be seen from Fig. 3a where we show the net shortwave radiation flux, the longwave radiation flux, and the sum of the sensible and latent heat for summer and winter, respectively. During winter there is a large ocean energy flux into the atmosphere. This is due to the large turbulent fluxes of sensible and latent heat as well as to the large net longwave radiation from the relatively warm ocean regions. The net surface energy flux over land is much smaller. In this case the radiation losses are compensated by atmospheric heat transfer and to a minor degree by a net positive flux of mainly sensible heat directed from the atmosphere to land. During summer the situation is reversed and both land and ocean regions constitute an energy sink for the atmosphere driven by the huge surplus of solar radiation, which dominates over the net longwave radiation. The ocean warming is considerable, reaching a value of almost -95 W m^{-2} in June. In comparison the net surface flux over land areas is smaller because of the large latent heat flux (high evaporation) and longwave radiation that removes energy from the land surface.

The seasonal variation of the residual (*dE/dt)* (Table 1; Fig. 2a) is positive in the first part of the year and negative in the second with a peak at the equinoxes. This variation is due to the seasonal changes of the energy (temperature and water vapor) of the atmospheric column. There is a small annual deficit of -1.7 W m^{-2}, which could be related to the fact that we have not included the transport of kinetic energy and possibly to minor rounding errors in the calculations.

We have also compared the top-of-atmosphere net outgoing radiation with measurements from CERES (Wielicki et al. 1996) for the period 2001–09. The observations do not coincide in time with the model data but this is of minor importance as we are here only comparing the annually averaged values. Even if the model is forced by observed greenhouse gases and aerosols it cannot reproduce the observed individual annual values. The results show that there is a good agreement in the annual mean as can be seen from Fig. 4a but with relatively large differences in summer with a too high reflected shortwave

Brought to you by MAX-PLANCK-INSTITUTE FOR METEOROLOGY | Unauthenticated | Downloaded 04/11/23 01:41 PM UTC

TABLE 1. Annual cycle of components of the energy budget in the NPR and the SPR for the T213 model 20C period. Units are W m^{-2}, ± values indicate the 95% confidence intervals.

	Lq	$C_pT + gZ$	F_{WALL}	F_{SFC}	F_{RAD}	dE/dt
			Northern Hemisphere			
Jan	17.1 ± 0.9	103.6 ± 5.0	120.7 ± 4.9	53.6 ± 1.5	−170.7 ± 0.8	3.6
Feb	18.1 ± 1.1	103.6 ± 5.7	121.7 ± 5.8	47.6 ± 1.6	−157.0 ± 0.7	12.3
Mar	18.2 ± 0.9	85.5 ± 4.1	103.7 ± 4.3	32.1 ± 1.2	−124.9 ± 0.5	10.9
Apr	18.7 ± 0.8	73.1 ± 3.7	91.8 ± 3.8	3.0 ± 0.8	−72.0 ± 0.5	22.8
May	17.2 ± 1.0	42.6 ± 2.9	59.8 ± 2.8	−33.4 ± 0.5	−5.4 ± 0.5	21.0
Jun	17.6 ± 1.0	25.0 ± 2.0	42.6 ± 1.9	−56.5 ± 0.6	30.4 ± 1.0	16.5
Jul	21.6 ± 1.1	18.1 ± 1.9	39.7 ± 2.0	−52.3 ± 0.5	7.7 ± 1.0	−4.9
Aug	27.6 ± 0.9	29.2 ± 2.3	56.7 ± 1.9	−23.3 ± 0.6	−55.9 ± 0.6	−22.5
Sep	28.2 ± 1.2	47.5 ± 3.0	78.1 ± 2.8	13.4 ± 0.8	−119.7 ± 0.4	−28.2
Oct	26.4 ± 1.1	64.1 ± 3.6	90.6 ± 3.6	42.8 ± 1.1	−163.6 ± 0.4	−30.2
Nov	21.6 ± 1.2	83.3 ± 4.7	104.8 ± 4.6	55.2 ± 1.3	−177.7 ± 0.5	−17.7
Dec	19.0 ± 1.1	99.6 ± 4.2	118.6 ± 4.5	55.5 ± 1.6	−175.7 ± 0.6	−1.6
Annual	20.9 ± 0.3	64.6 ± 0.8	85.5 ± 0.9	11.5 ± 0.4	−98.7 ± 0.2	−1.7
			Southern Hemisphere			
Jan	23.7 ± 1.0	31.5 ± 2.4	55.3 ± 2.1	−72.4 ± 0.8	12.8 ± 0.7	−4.3
Feb	26.3 ± 0.9	33.2 ± 2.9	59.5 ± 2.9	−28.3 ± 0.7	−46.4 ± 0.6	−15.2
Mar	30.2 ± 0.9	41.1 ± 3.5	71.3 ± 3.3	18.1 ± 0.9	−109.1 ± 0.4	−19.7
Apr	31.3 ± 0.9	55.7 ± 5.2	87.0 ± 5.3	49.0 ± 1.1	−151.4 ± 0.5	−15.4
May	30.2 ± 0.9	62.3 ± 4.6	92.5 ± 4.7	60.4 ± 1.1	−166.7 ± 0.5	−13.8
Jun	29.5 ± 1.0	70.3 ± 4.6	99.8 ± 4.8	58.4 ± 1.4	−167.6 ± 0.6	−9.4
Jul	28.3 ± 1.0	77.5 ± 4.3	105.8 ± 4.2	56.1 ± 1.2	−162.8 ± 0.6	−0.9
Aug	29.3 ± 0.8	77.1 ± 4.4	106.4 ± 4.3	46.6 ± 1.2	−150.2 ± 0.6	2.8
Sep	29.1 ± 0.7	71.7 ± 4.8	100.7 ± 4.6	29.4 ± 0.9	−120.7 ± 0.5	9.4
Oct	27.8 ± 0.8	64.0 ± 4.1	91.8 ± 4.1	−1.9 ± 1.0	−71.2 ± 0.9	18.7
Nov	25.7 ± 1.0	49.9 ± 4.3	75.6 ± 4.0	−47.1 ± 1.3	−10.4 ± 1.5	18.1
Dec	22.8 ± 0.8	37.2 ± 2.7	60.0 ± 2.8	−82.5 ± 1.3	30.6 ± 1.1	8.1
Annual	28.0 ± 0.3	56.3 ± 0.9	84.3 ± 0.9	8.0 ± 0.4	−92.2 ± 0.3	−1.1

radiation that occurs both over land and ocean. Over land the modeled net outgoing longwave radiation is underestimated both for summer and winter probably as a result of the model temperatures being too low. As can be seen from Fig. 5a, the difference in the reflected shortwave radiation in summer is due to a too high model albedo.

b. The SPR

For the SPR (bottom part of Table 1; Fig. 2b) the annual mean of the moist heat transport (Lq) is some 34% larger than in the NPR presumably because of the proportionally much larger ocean area of the Southern Hemisphere. The annual variability is also smaller reflecting the stronger similarity of the atmospheric circulation between summer and winter in the Southern Hemisphere. At the same time the annual mean transport of dry static energy is smaller and so is its annual variability (Table 1). Interestingly, the annual mean of the total atmospheric energy transport F_{WALL} for both polar regions is almost the same. However, the peak transport of dry static energy for the SPR winter is markedly weaker than the winter maximum of the NPR. We suggest that this is due to differences in the character of the general circulation at the high latitudes of the two hemispheres with the SH more dominated by transient disturbances moving in the dominant westerly storm track, while the NH has more marked storm tracks oriented southwest–northeast, in particular in the Atlantic sector, that are more efficient in transporting energy into the NPR. This is particularly marked in the Norwegian Sea sector with its strong maximum of moist energy transport across 60°N (Bengtsson et al. 2011a).

The seasonal variation of the residual (dE/dt) in the SPR is positive from August to December and negative from January to July with the largest changes found around the equinoxes. As for the NPR the variation is due to the seasonal changes of the energy (temperature and water vapor) of the atmospheric column. Because of the reduced amplitude of atmospheric temperature in the SPR the amplitude is less than for the NPR. There is a small annual deficit of −1.1 W m^{-2} that as already stated could be related to the fact that the transport of kinetic energy is not included in the budget.

Brought to you by MAX-PLANCK-INSTITUTE FOR METEOROLOGY | Unauthenticated | Downloaded 04/11/23 01:41 PM UTC

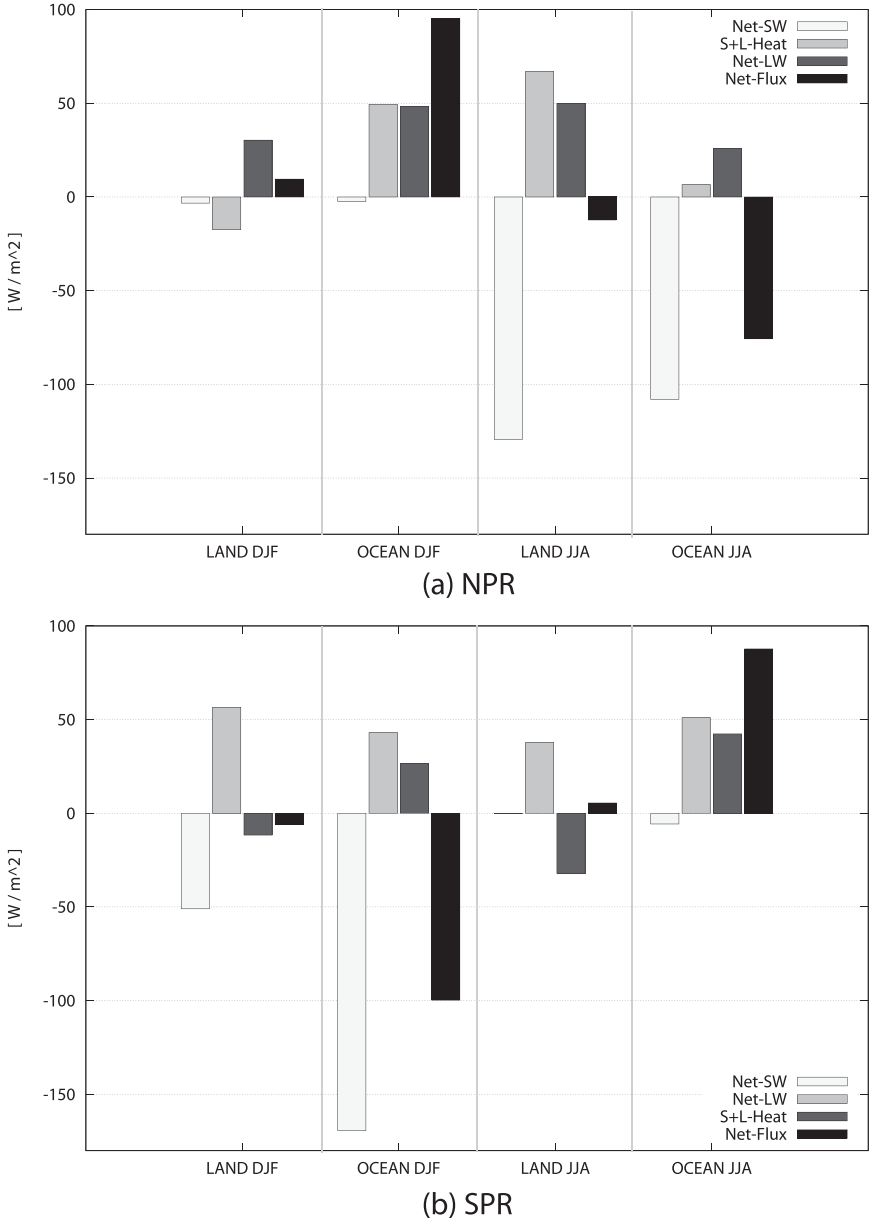

FIG. 3. Surface energy fluxes of net shortwave and longwave radiation and the sum of the sensible and latent heat fluxes for winter and summer for (a) the NPR and (b) the SPR for the 20C period. Units are W m^{-2}.

The net surface energy fluxes F_{SFC} (Table 1) undergo very large seasonal variations that are some 25% larger that for the NPR but the annual average is rather small and in fact smaller than what is seen in the NPR. The individual components of the surface energy balance for the SPR for summer [December–February (DJF)] and winter [June–August (JJA)] and for land and ocean separately are also shown in Fig. 3b. The net shortwave radiation in the summer is particularly large and negative over the ocean, which means a corresponding ocean heat gain, but this is partially offset by the surface energy fluxes and net longwave cooling. The result is a net surface heat flux from the atmosphere to land. In the SPR winter the net shortwave radiation is almost insignificant but there is a strong net surface ocean energy flux to the atmosphere. Over the Antarctic land–ice the differences are minor between summer (DJF) and winter (JJA). The strong reversed heat flux in JJA of 32.1 W m^{-2} almost fully offsets the net longwave surface cooling.

Brought to you by MAX-PLANCK-INSTITUTE FOR METEOROLOGY | Unauthenticated | Downloaded 04/11/23 01:41 PM UTC

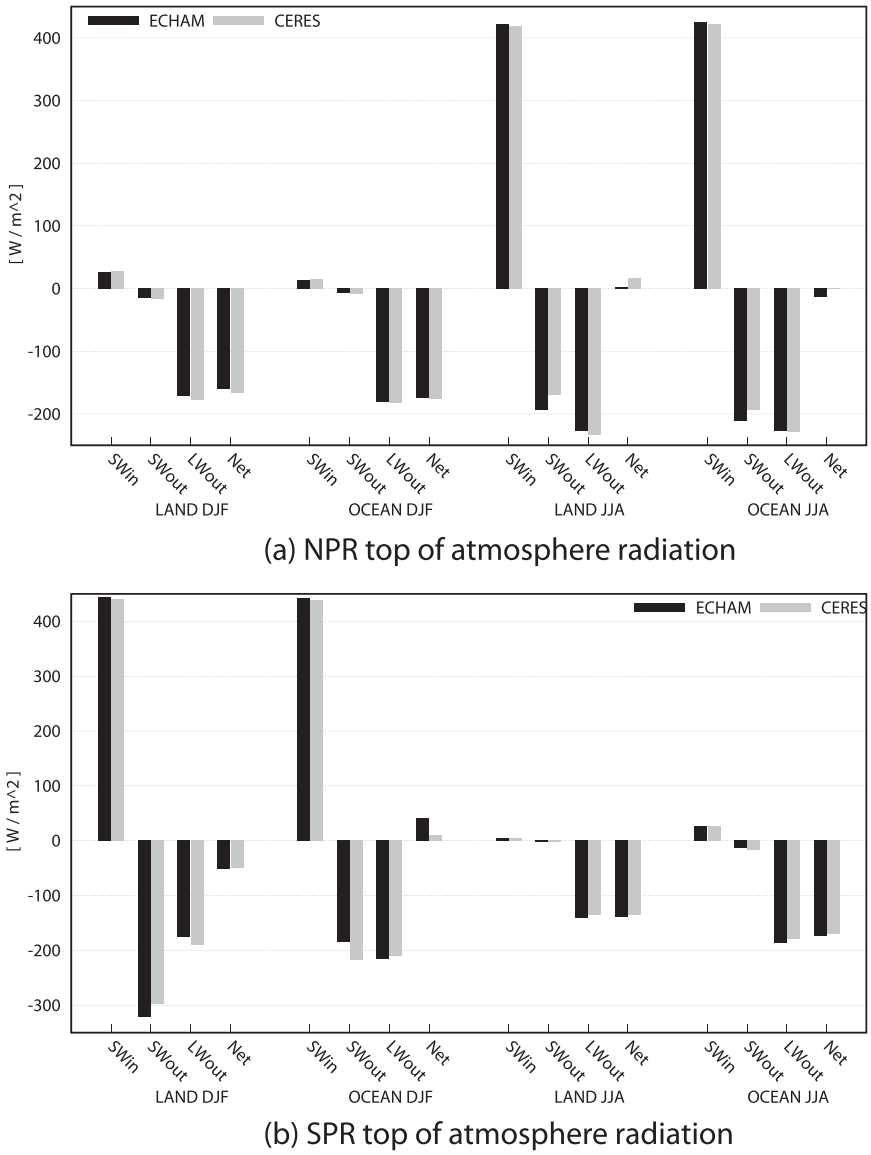

FIG. 4. Top-of-atmosphere radiation in (a) NPR (b) SPR, for CERES and the model 20C period. Units are W m^{-2}.

As for the NPR we have compared the top-of-the-atmosphere radiation with data from CERES, (Fig. 4b). The comparison shows large differences over the oceans in the summer (DJF). Here the CERES albedo data are significantly larger than the model albedo values (Fig. 5b) and for the annual average by some 17%. We tentatively suggest that a likely reason for the lower albedo of the model is too little cloud in the model simulation. Similar results have been reported by other studies (Trenberth and Fasullo 2010; Haynes et al. 2011). The reason for this is not clear but seems to be related to an underestimation by models of midlevel clouds (Zhang et al. 2005). However, the CERES data are probably less reliable over the Antarctic continent owing to the high latitude and the general problem of separating boundary layer clouds from the snow and ice covered surface. The model data here have slightly higher albedo values than reported from CERES.

Finally in comparing the two polar regions we note from Table 2 that the energy lost to space, based on the CERES data, is almost the same or 97 W m^{-2} for both polar regions, although this is composed differently between the land and ocean for the two polar regions. For the NPR the model data agree well with CERES both for land and ocean separately; however, for the SPR there is a considerable disagreement, in particular for

Brought to you by MAX-PLANCK-INSTITUTE FOR METEOROLOGY | Unauthenticated | Downloaded 04/11/23 01:41 PM UTC

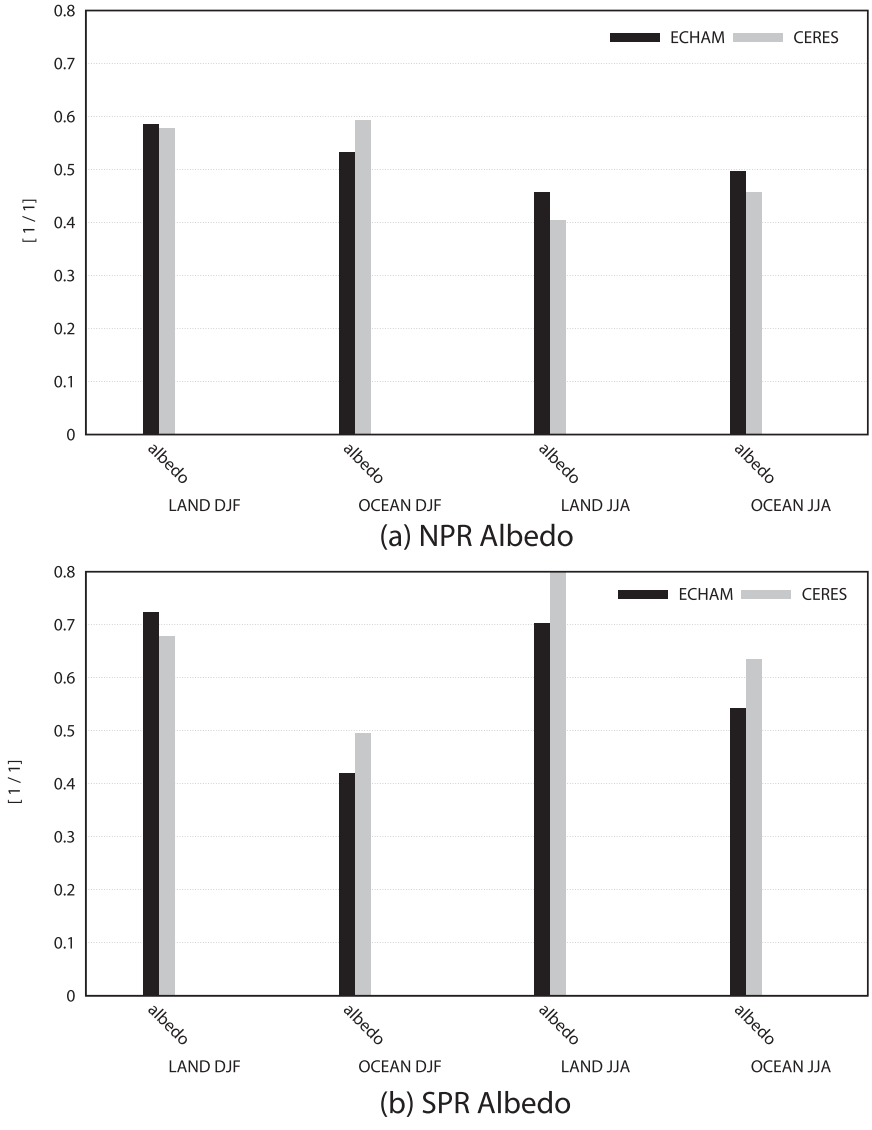

FIG. 5. Albedo for CERES and the model 20C period: (a) NPR and (b) SPR.

the ocean region where the model underestimates F_{RAD} while over land the model overestimates F_{RAD}. The combined loss of energy to space is some 4 W m^{-2} less mainly because of the much smaller energy loss over the SPR ocean areas.

4. Polar energy fluxes in a warmer climate

The evaluation of the climate change simulation compares the 20C with the 21C experiments. The result of the transport calculations and the vertical energy fluxes for 21C are summarized in Table 3 where we show the monthly mean values averaged for the 30-yr period for NPR and SPR, respectively, the 95% confidence intervals are included for selected parameters calculated from the standard error of the interannual variability. As can be seen from Table 3 the total horizontal transport has changed little in both the NPR and SPR but there has been a reduction of the dry static energy

TABLE 2. Annual-average top-of-atmosphere total net radiation balance for the two polar regions. Observations from CERES for the years 2001–09, and from the model for the period 1960–90. Units are W m^{-2}.

	NPR		SPR	
	CERES	ECHAM5	CERES	ECHAM5
Total	−97.0	−98.3	−97.0	−92.8
Land	−88.9	−89.9	−101.6	−108.3
Ocean	−104.9	−106.5	−94.0	−82.2

Brought to you by MAX-PLANCK-INSTITUTE FOR METEOROLOGY | Unauthenticated | Downloaded 04/11/23 01:41 PM UTC

TABLE 3. Annual cycle of components of the energy budget in the NPR and the SPR for the T213 model 21C period. Units are W m^{-2}, ± values indicate the 95% confidence intervals.

	Lq	$C_pT + gZ$	F_{WALL}	F_{SFC}	F_{RAD}	dE/dt
			Northern Hemisphere			
Jan	23.1 ± 1.5	100.5 ± 5.4	123.5 ± 5.3	57.1 ± 1.8	−177.4 ± 0.7	3.2
Feb	22.1 ± 1.1	95.9 ± 6.4	118.9 ± 6.6	49.4 ± 1.5	−162.6 ± 0.6	4.8
Mar	22.5 ± 1.2	82.0 ± 4.5	104.5 ± 4.7	31.1 ± 1.3	−126.0 ± 0.6	9.6
Apr	23.3 ± 0.9	68.6 ± 3.3	92.0 ± 3.3	−3.7 ± 1.1	−66.2 ± 0.6	22.1
May	21.1 ± 1.1	40.3 ± 2.1	61.4 ± 2.2	−42.4 ± 0.7	1.9 ± 0.8	20.9
Jun	23.0 ± 0.9	23.1 ± 2.2	46.1 ± 2.1	−67.9 ± 0.8	39.0 ± 1.4	17.2
Jul	28.3 ± 1.2	15.6 ± 2.2	43.9 ± 2.2	−62.6 ± 0.9	15.2 ± 1.3	−3.5
Aug	34.1 ± 1.1	24.1 ± 2.7	58.2 ± 2.2	−30.0 ± 0.8	−54.6 ± 0.8	−26.4
Sep	38.4 ± 1.3	39.8 ± 2.7	78.1 ± 2.5	12.3 ± 0.8	−123.6 ± 0.4	−33.2
Oct	34.9 ± 1.3	55.4 ± 3.5	90.3 ± 3.2	44.5 ± 1.4	−168.9 ± 0.3	−34.3
Nov	29.1 ± 1.4	71.5 ± 4.2	100.7 ± 4.2	59.3 ± 1.6	−185.2 ± 0.5	−25.2
Dec	24.8 ± 1.3	89.8 ± 4.8	114.6 ± 4.6	61.5 ± 1.8	−183.7 ± 0.6	−7.6
Annual	27.0 ± 0.4	58.9 ± 1.2	85.9 ± 1.3	9.1 ± 0.5	−99.3 ± 0.3	−4.3
			Southern Hemisphere			
Jan	29.8 ± 1.0	25.7 ± 3.1	55.6 ± 3.1	−71.8 ± 0.5	13.0 ± 0.8	−3.2
Feb	34.6 ± 1.0	24.8 ± 2.3	59.5 ± 2.3	−27.4 ± 0.8	−49.0 ± 0.8	−16.9
Mar	39.8 ± 0.9	38.3 ± 7.2	78.2 ± 7.3	17.0 ± 0.8	−110.1 ± 0.5	−14.9
Apr	39.2 ± 1.2	47.1 ± 4.3	86.2 ± 4.2	45.8 ± 1.1	−151.8 ± 0.5	−19.8
May	37.7 ± 0.9	55.5 ± 5.0	93.2 ± 5.2	57.9 ± 1.2	−166.4 ± 0.4	−15.3
Jun	35.0 ± 1.1	57.9 ± 4.1	92.9 ± 4.2	59.2 ± 1.2	−166.6 ± 0.5	−14.5
Jul	33.7 ± 0.9	74.4 ± 4.3	108.0 ± 4.1	56.2 ± 1.0	−163.1 ± 0.6	1.1
Aug	32.7 ± 1.0	67.7 ± 4.7	100.5 ± 4.5	47.1 ± 1.1	−149.2 ± 0.5	−1.6
Sep	32.5 ± 1.1	60.8 ± 5.1	93.2 ± 5.0	26.7 ± 1.1	−115.0 ± 0.5	4.9
Oct	33.4 ± 1.1	49.2 ± 3.0	82.5 ± 3.0	−11.7 ± 0.9	−59.5 ± 0.8	11.3
Nov	31.2 ± 0.9	39.4 ± 3.7	70.6 ± 3.7	−59.9 ± 1.0	3.8 ± 0.8	14.5
Dec	29.0 ± 1.0	32.0 ± 3.0	61.0 ± 3.0	−88.9 ± 0.7	37.8 ± 0.9	9.9
Annual	34.0 ± 0.5	47.7 ± 1.3	81.8 ± 1.4	4.2 ± 0.4	−89.7 ± 0.3	−3.7

and a corresponding increase in the moist energy transport of ~6%.

We illustrate this further in Fig. 6, which depicts the scatterplot of the transport of moisture (latent heat) versus the transport of dry static energy into the polar regions for each individual year of the experiments. The increase in moist heat transport is very clear and for every single year the transport for 21C is larger than any of the years for 20C, this is true for both polar regions. The dry static energy is also smaller in 21C for most years but the mean reduction stands out and so does the systematic difference between the two polar regions. The SPR has a larger moist heat transport but a smaller dry static transport than the NPR.

In Fig. 7 we show the vertical profile of the annual mean total energy transport across 60°N and 60°S, respectively. The total transport is dominated by the dry static energy as shown by the actual values shown in Table 3. While the moist energy transport is positive at all levels the net transport of dry static energy is positive in the lower troposphere but negative aloft. The dry static energy is much larger than the moist energy but only a minor part of the dry static energy is being delivered to the polar regions. In fact most of the energy is being returned to lower latitudes with a slightly reduced value. For 20C and 21C the patterns of net transport

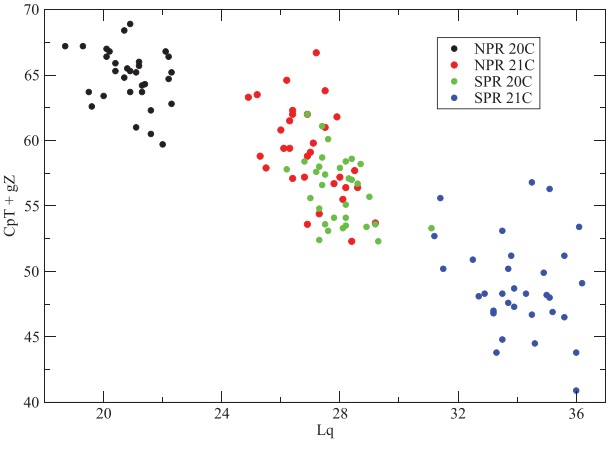

FIG. 6. Scatterplot of the annual transport of energy associated with moisture (Lq) vs the transport of dry static energy ($c_pT + gZ$). Units are W m^{-2}.

Brought to you by MAX-PLANCK-INSTITUTE FOR METEOROLOGY | Unauthenticated | Downloaded 04/11/23 01:41 PM UTC

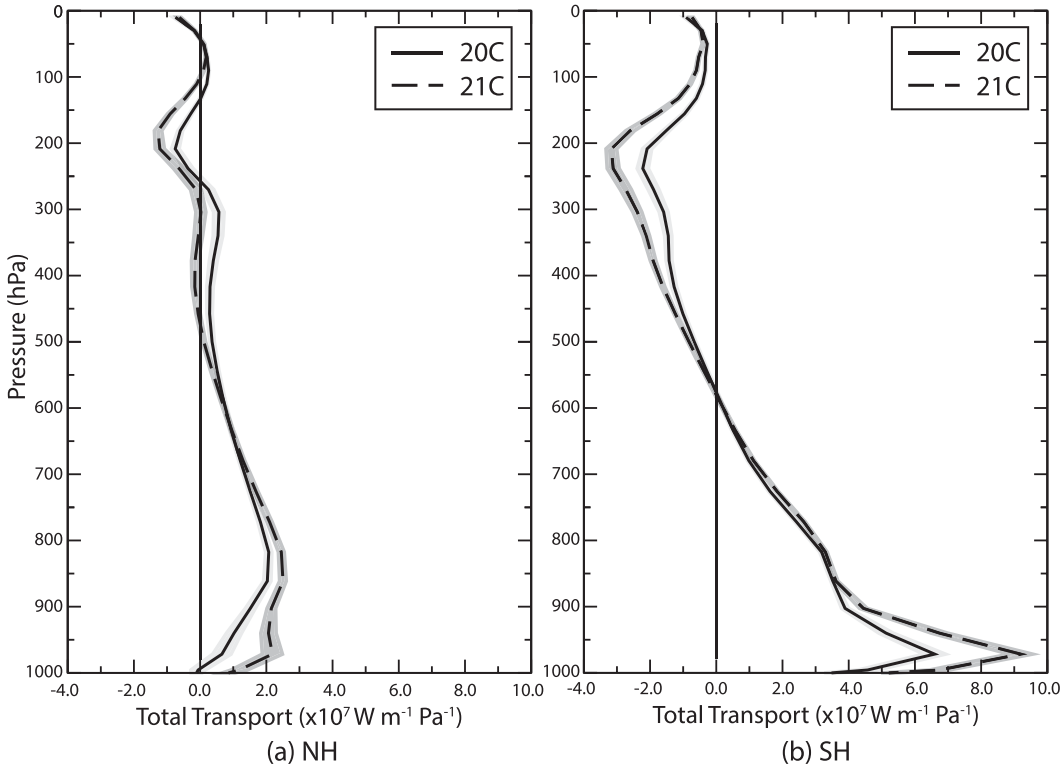

FIG. 7. Mean annual vertical profiles of total energy transport ($c_pT + gZ + Lq$) across 60°N and 60°S for 20C and 21C in the (a) NH and (b) SH. Pressure levels are nominal values. Energy transport units are W m^{-1} Pa^{-1}.

are similar but with slightly larger values for 21C. This does not indicate any major change in circulation in the vertical plane but is simply the result of the energy content being larger in 21C because of higher temperatures. As is clear from Table 3 and discussed elsewhere in this article the total net amount of energy transport is practically unchanged. The sharp maximum in the dry static energy transport in the boundary layer in the SPR region is related to the fact that 60°S is predominately over the ocean. For NPR 60°N is mainly over land and in many land regions at high altitude. This means that the energy transport takes place at higher elevation and consequently at lower pressure. This highlights the need to perform the calculations in model coordinates.

We have also examined the moist and dry energy transport as a function of longitude (Fig. 8). The net dry static energy is composed of areas of high energy inflow as well as of areas of high energy outflow. The size of the regions of maximum inflow and outflow is ~2 orders of magnitude larger than the moist transport. This requires accurate and consistent data and is consequently difficult to do directly from analyzed datasets. To do it from a model as in this case has the advantage that the data are dynamically and physically consistent at every time. The largest inflow regions for both moist and dry transport occur at the end of the storm tracks in the NH and in the Indian and Pacific Oceans in the SH. This is consistent with the penetration of the storm tracks into the polar regions.

a. The NPR

The energy fluxes for NPR for 21C are shown in the top half of Table 3 (monthly values) and in Fig. 9a for each season. The transition from dry static energy transport to moist heat energy transport can be found for each season and with only minor changes in the total transport across 60°N. Similarly, the energy loss to space is also practically identical with a slight increase in winter and autumn and a corresponding reduction in spring and summer. The difference is related to a larger energy transfer into the ocean in spring and summer and a corresponding gain in winter and autumn. The enhanced seasonal cycle in the energy exchange with the oceans is mainly related to the loss of sea ice during the summer (not shown).

The total energy transport across 60°N for 20C amounts to 120.4 W m^{-2} and is similar for the three winter months. It is dominated by the transport of dry static energy. The

Brought to you by MAX-PLANCK-INSTITUTE FOR METEOROLOGY | Unauthenticated | Downloaded 04/11/23 01:41 PM UTC

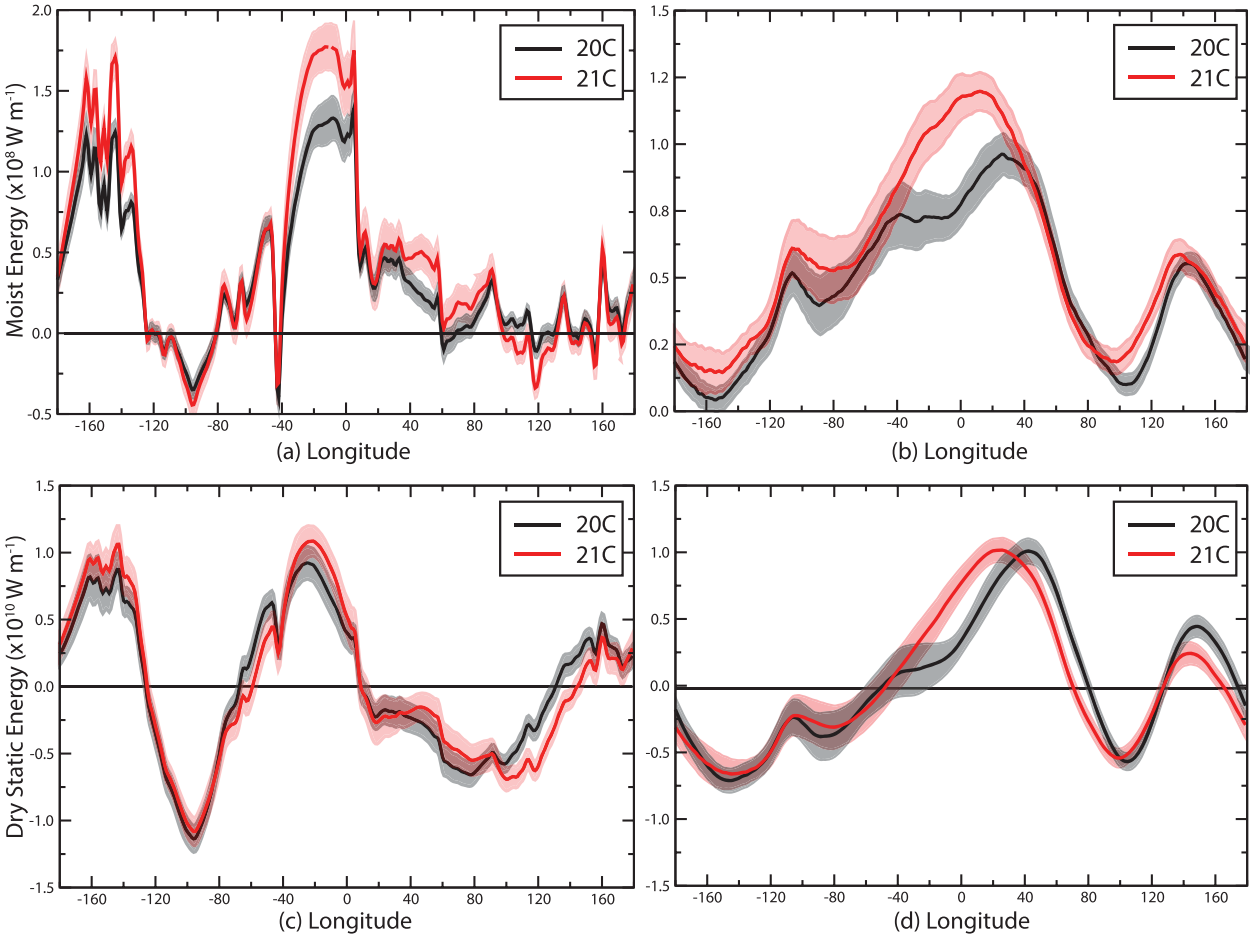

FIG. 8. Mean annual transport of energy as a function of longitude across 60°N and 60°S associated with moisture and dry static energy for 20C and 21C: (a) NH moisture, (b) SH moisture, (c) NH dry static, and (d) SH dry static. Units are W m^{-1}.

net energy flux from the surface is large, with 52.2 W m^{-2}. It is dominated by the flux from the ocean, with almost equally large contributions of net longwave radiation and fluxes of latent and sensible heat. The net latent heat flux over land also contributes to warm the atmosphere but with a much smaller value while the fluxes of sensible and latent heat are reversed and directed from the atmosphere to the land. The huge atmospheric energy gain through horizontal and vertical transport is radiated into space illustrating the efficiency of the polar regions to get rid of the surplus energy transported into the region as well as the heat extracted from the surface. A small energy gain of 4.7 W m^{-2} is due to atmospheric warming at the end of the winter season.

For 21C the total horizontal energy transport during winter is about the same as for 20C but the moist energy increases by 5.2 W m^{-2} while the dry energy diminishes by 6.9 W m^{-2}. As will be discussed later this is an expected change in a warmer climate (Held and Soden 2006). The heat transfer from the surface increases because of enhanced energy fluxes of mainly latent heat from the ocean. There is virtually no net energy being stored in the system and the full amount of 174.6 W m^{-2} disappears into space.

During summer the situation is different. The horizontal energy transport for 20C is reduced to ~⅓ of the wintertime total transport and the moist transport is almost as large as the dry energy transport. There is only a small cooling to space because of the contribution during August whereas in June and July the NPR has a positive radiation balance (there is more incoming than outgoing radiation). The surplus of energy warms the ocean by as much as 75.7 W m^{-2} (Table 4).

For 21C the moist energy transport dominates and is in fact larger than the dry transport by more than ⅓. As during winter the dry static energy transport decreases by a similar amount. There is a significant net increase in

Brought to you by MAX-PLANCK-INSTITUTE FOR METEOROLOGY | Unauthenticated | Downloaded 04/11/23 01:41 PM UTC

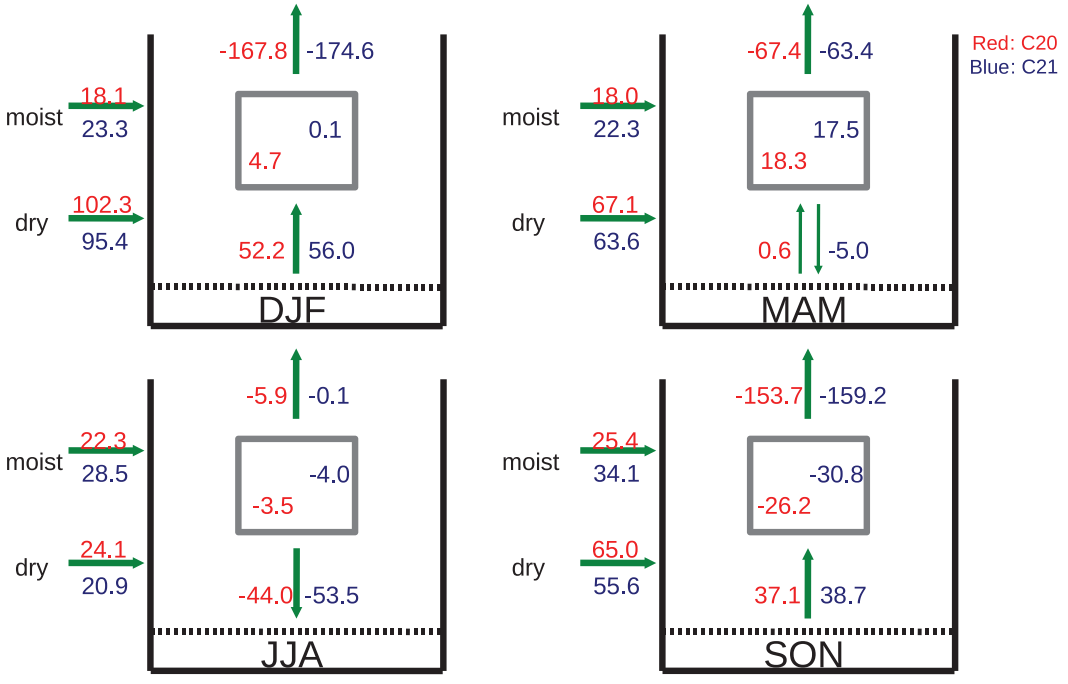

(a) NPR Energy Fluxes

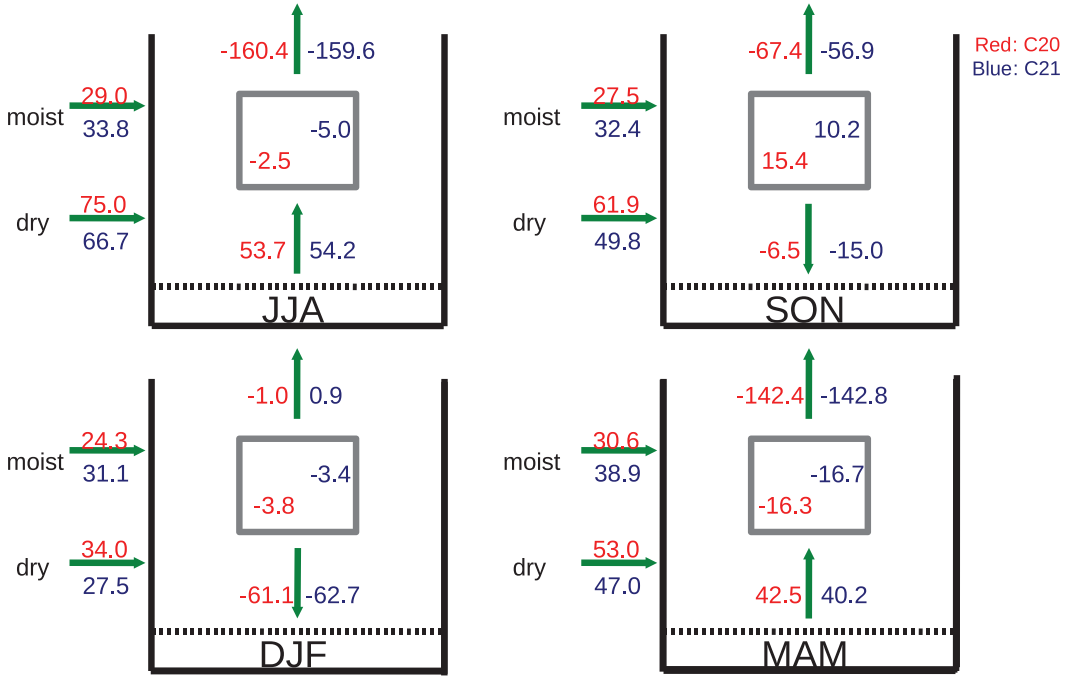

(b) SPR Energy Fluxes

FIG. 9. Seasonal energy fluxes for (a) the NH and (b) the SH. Units are W m^{-2}. The boxes indicate the atmospheric volume poleward of 60°. The arrows indicate the direction of the energy flux and the numbers the amount in W m^{-2} averaged over the polar region.

Brought to you by MAX-PLANCK-INSTITUTE FOR METEOROLOGY | Unauthenticated | Downloaded 04/11/23 01:41 PM UTC

TABLE 4. Surface energy balance for winter and summer, land and ocean and for 20C and 21C (parentheses).

	DJF		JJA	
	Land	Ocean	Land	Ocean
		NPR		
Net SW	3.3 (3.4)	2.4 (2.8)	129.3 (127.3)	108.0 (116.8)
Net LW	−30.3 (−29.2)	−48.3 (−48.2)	−50.0 (−45.8)	−25.8 (−18.0)
Sensible + latent heat	17.5 (17.0)	−49.4 (−58.2)	−67.0 (−68.6)	−6.5 (−5.3)
Net surface flux	−9.5 (−8.8)	−95.3 (−103.6)	12.3 (12.9)	75.7 (93.5)
		SPR		
Net SW	51.0 (50.3)	169.3 (163.3)	0.2 (0.2)	5.7 (6.5)
Net LW	−56.6 (−53.9)	−43.1 (−36.1)	−37.8 (−36.4)	−51.0 (−48.4)
Sensible + latent heat	11.6 (10.1)	−26.5 (−25.5)	32.1 (30.8)	−42.4 (−45.7)
Net surface flux	6.5 (6.0)	99.7 (101.7)	−5.5 (−5.3)	−87.7 (−87.6)

the transport of energy into the ocean. This is mainly a consequence of increased solar radiation absorbed at the surface but also to a reduced longwave radiation cooling (Table 4). The outgoing longwave radiation from the surface increases because of the higher surface temperatures, but the downward longwave radiation increases more as the atmosphere is getting both warmer and more humid.

As can be seen from Fig. 9a the transitional seasons are different. For 21C the moist energy transport increases in the autumn by a significant amount and the dry static energy transport correspondingly decreases. There is a net accumulation of energy in the spring when the system is warming up (see Table 3) and a net energy loss in autumn when the system is cooling.

Based on the different energy components we suggest the following mechanism for the Arctic climate. The horizontal transport of energy is broadly conserved but changes character as proportionally more energy is transported in the form of moist energy and correspondingly less as dry energy. The increased amount of moisture transported into the polar region is probably a major reason why the net radiative surface cooling is being reduced. This is more noticeable in summer when the moisture transport is large. The reason that the solar radiation increases is probably due to reduced ice cover. The increase in net solar radiation at the surface and a corresponding reduction in longwave cooling leads to a massive increase in the net surface flux by some 18 W m^{-2} (Table 4). Part of this surplus heat is being returned to the atmosphere during the late autumn and winter.

b. The SPR

Figure 9b depicts the energy balance for the SPR for both the 20C and 21C. The total energy transport in the SH winter (JJA) is some 86% of the transport into the NPR. The situation is reversed during the SH summer (DJF) when the total energy transport is larger than for NPR so that the mean value for the whole year is similar (see Table 3). The proportion of moist energy transport is also significantly larger than for NPR. This can be explained by the different surface properties in the SH to those in the NH. There is much more ocean at the bottom boundary in the SH, which can provide more moisture to the atmosphere through evaporation. The results for 21C are similar with the difference that the proportion of moist energy transport is larger. Even during the SH winter the moist transport is more than 50% of the dry static energy transport with an even larger proportion for the other seasons. Generally the changes in the total energy balance between 20C and 21C for the SPR are minor. The annual net surface flux is reduced from 8.0 to 4.3 W m^{-2} but this is against a huge annual cycle with an amplitude of some 75 W m^{-2} (Table 3). An inspection of the surface energy fluxes over land and ocean separately (Table 4) also shows very modest changes.

5. Discussion and concluding remarks

The polar energy fluxes for both hemispheres and for two 30-yr periods have been calculated by a high-resolution climate model for the end of the twentieth and twenty-first centuries using the IPCC A1B scenario. The short- and longwave radiation fluxes agree well with CERES data for the 20C and NPR, but for the SPR the albedo is underestimated over the oceans leading to an overly strong solar radiation at the surface.

The total energy transport is broadly unchanged, but for the NPR there is an increase in the moist energy transport by ~6 W m^{-2} and a corresponding reduction in the dry static energy. The result for the SPR is the

Brought to you by MAX-PLANCK-INSTITUTE FOR METEOROLOGY | Unauthenticated | Downloaded 04/11/23 01:41 PM UTC

TABLE A1. Annual cycle of components of the energy budget in the NPR and the SPR for the T63 model 20C period. Units are W m^{-2}, ± values indicate the 95% confidence intervals.

	Lq	$C_pT + gZ$	F_{WALL}	F_{SFC}	F_{RAD}	dE/dt
			Northern Hemisphere			
Jan	17.9 ± 0.9	105.2 ± 7.9	123.1 ± 8.1	49.3 ± 1.4	−167.8 ± 0.7	4.6
Feb	18.3 ± 1.2	94.5 ± 3.8	112.8 ± 3.6	43.8 ± 1.0	−153.4 ± 0.7	3.2
Mar	19.4 ± 1.1	94.6 ± 4.0	114.0 ± 3.7	29.7 ± 0.9	−123.8 ± 0.6	2.0
Apr	19.4 ± 0.9	77.5 ± 2.6	96.9 ± 2.7	5.2 ± 0.8	−76.8 ± 0.5	25.1
May	19.4 ± 1.2	51.6 ± 3.2	71.0 ± 2.9	−23.8 ± 0.6	−22.6 ± 0.5	24.6
Jun	19.3 ± 0.9	31.3 ± 1.9	50.6 ± 2.0	−42.1 ± 0.8	8.7 ± 1.0	17.2
Jul	22.9 ± 1.1	27.2 ± 2.1	50.1 ± 2.4	−43.1 ± 0.7	−5.7 ± 1.4	1.3
Aug	26.4 ± 1.1	35.7 ± 2.5	62.1 ± 2.4	−17.2 ± 0.7	−63.5 ± 0.7	−1.9
Sep	29.4 ± 1.3	49.5 ± 3.5	78.9 ± 3.2	15.3 ± 0.9	−121.4 ± 0.5	−27.2
Oct	26.5 ± 1.1	70.8 ± 3.5	97.3 ± 3.6	40.2 ± 1.1	−161.0 ± 0.4	−23.5
Nov	23.0 ± 1.1	84.9 ± 5.2	107.9 ± 5.4	52.0 ± 1.4	−174.1 ± 0.5	−14.2
Dec	18.8 ± 1.5	99.2 ± 6.4	118.0 ± 6.9	52.2 ± 1.5	−172.9 ± 0.7	−2.7
Annual	21.7 ± 0.3	68.5 ± 1.1	90.2 ± 1.1	13.4 ± 0.3	−102.9 ± 0.2	0.7
			Southern Hemisphere			
Jan	21.1 ± 0.8	33.8 ± 3.5	54.9 ± 3.5	−61.8 ± 0.7	3.1 ± 0.8	−3.8
Feb	25.2 ± 0.7	36.1 ± 2.6	61.3 ± 2.6	−24.0 ± 0.7	−50.6 ± 0.8	−13.3
Mar	27.8 ± 1.1	41.3 ± 5.6	69.1 ± 5.3	19.7 ± 1.0	−109.6 ± 0.5	−20.8
Apr	30.5 ± 0.8	59.6 ± 3.7	90.1 ± 3.4	49.1 ± 0.9	−149.8 ± 0.4	−10.6
May	29.1 ± 1.0	70.7 ± 4.9	99.8 ± 4.5	58.8 ± 0.9	−165.2 ± 0.4	−6.6
Jun	27.0 ± 0.9	76.8 ± 5.2	103.8 ± 5.3	58.9 ± 1.3	−166.3 ± 0.5	−3.6
Jul	26.9 ± 0.8	85.1 ± 5.3	112.0 ± 5.4	54.6 ± 1.3	−162.0 ± 0.6	4.6
Aug	28.0 ± 0.8	79.7 ± 4.8	107.7 ± 4.5	45.1 ± 1.4	−149.6 ± 0.6	3.2
Sep	27.8 ± 0.8	84.1 ± 4.3	111.9 ± 4.2	27.7 ± 1.0	−122.0 ± 0.7	17.6
Oct	26.2 ± 0.8	68.3 ± 4.1	94.5 ± 3.9	−1.0 ± 0.8	−75.3 ± 1.3	18.2
Nov	23.2 ± 0.9	62.4 ± 4.1	85.6 ± 4.0	−40.8 ± 1.5	−18.0 ± 1.8	26.8
Dec	19.3 ± 1.3	44.1 ± 4.1	63.4 ± 3.9	−70.2 ± 1.5	18.8 ± 1.7	12.0
Annuial	26.0 ± 0.4	61.8 ± 1.3	87.8 ± 1.4	9.7 ± 0.4	−95.6 ± 0.4	2.0

same but the proportion of moist energy transport is larger and the dry static energy smaller both for the present and the future climate.

The result is in broad agreement with the theoretical and model results reported by Held and Soden (2006). The expected increase in high-latitude precipitation with increased global temperature must be kept in mind when estimating the surface mass balance of the land ice and high-latitude mountain glaciers (Bengtsson et al. 2011b).

We further suggest that a possible mechanism for the warming of the Arctic Ocean is that as global temperatures increase the transport of water vapor across 60°N also increases. This results in an increase of the atmospheric opacity reducing the net surface longwave cooling. At the same time because of positive albedo feedback the amount of surface solar radiation absorption increases and the two radiation fluxes consequently work in the same direction. Comparing the change for 21C the net surface ocean radiation flux in summer increases by as much as 18 W m^{-2} or by 24%. For the SPR the response is different as here there is rather a decrease in shortwave solar radiation. We suggest that this is caused primarily by a more poleward storm track (Bengtsson et al. 2006, 2009) and associated cloudiness and minor changes in the summer sea ice as even in the present climate most of the winter sea ice melts during the summer. This is also what was found in the study of Zelinka et al. (2012) who demonstrated, using an ensemble of GCMs, that this enhanced reflection is a manifestation of both the poleward shift of the mid-latitude storm track and its attendant cloudiness as well as a brightening of clouds in subpolar regions, the latter being the dominant contributor. Further studies with other models and reanalyses are required to elucidate these issues.

It must be pointed out that the results presented here are from a single GCM only. However, we nevertheless have reasons to believe that the general result will be rather similar for other GCMs. The increase in the transport of water vapor across 60°N and 60°S with higher temperatures can easily be confirmed from precipitation calculations and was shown by Bengtsson et al. (2011b) to be the case. The net transport of heat and mass requires the availability of large quantities of high-frequency multilevel data and extensive calculations

Brought to you by MAX-PLANCK-INSTITUTE FOR METEOROLOGY | Unauthenticated | Downloaded 04/11/23 01:41 PM UTC

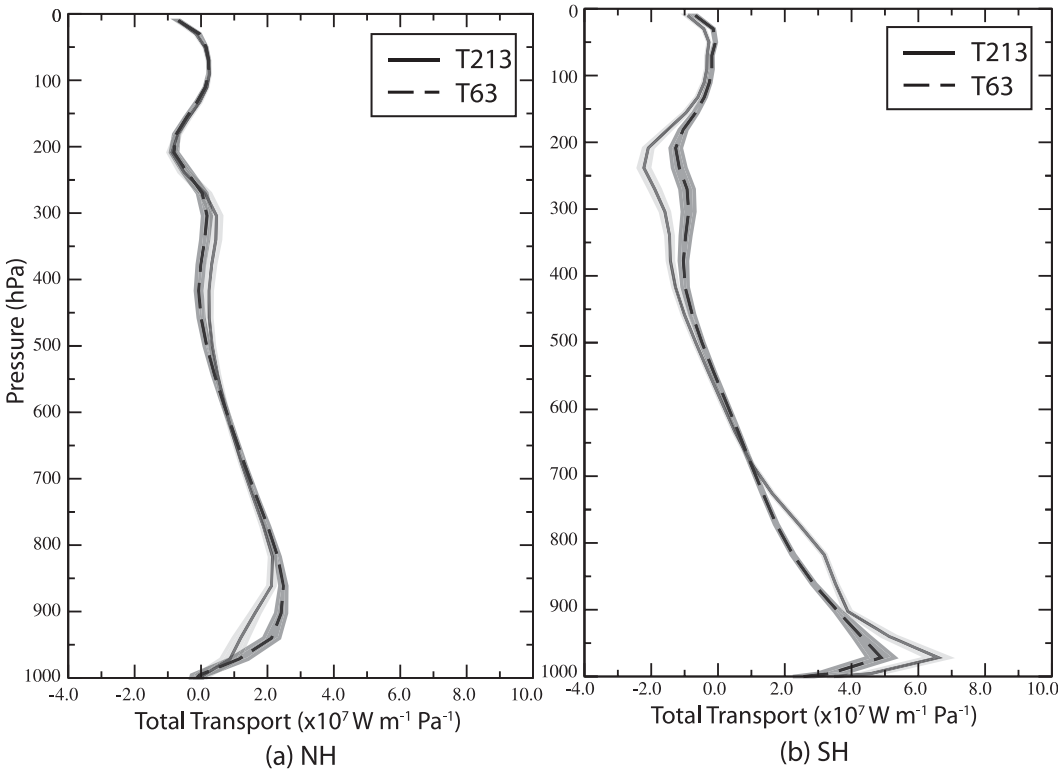

FIG. A1. Mean annual vertical profiles of total energy transport ($c_pT + gZ + Lq$) for T213 (solid line) and T63 (dashed line) in (a) the NH across 60°N and (b) the SH across 60°S. Pressure levels are nominal values. Energy transport units are W m^{-1} Pa^{-1}. The shading indicates the 95% confidence intervals.

and has not been possible to do for other models for this paper.

Finally the important question is whether the changes in the high-latitude water cycle can be observed. Reliable records for high-latitude precipitation for long periods hardly exist because of the sampling problems but long-term observations from countries with good precipitation networks such as Sweden suggest that an increase in annual precipitation over the last 50 years has taken place broadly following the increase in temperature. There are also indications from the Global Energy and Water Cycle Experiment (GEWEX) that arctic precipitation has been increasing in recent decades (G. Asrar 2012, personal communication).

Acknowledgments. The authors wish to thank the Max Planck Institute for Meteorology for making the ECHAM5 model available and Dr. Noel Keenlyside for running the simulations and making the data available. The simulations where performed at HLRN (Norddeutscher Verbund für Hoch und Höchstleistungsrechnen). Dr. Matthias Zahn was funded by the NERC PREPARE Project NE/G015708/1. The authors also want to thank the reviewers for their comments.

APPENDIX

Energy Balance for the T63 Coupled Model

The use of a high-resolution atmospheric model forced by lower-boundary conditions taken from a lower-resolution fully coupled simulation with the same model, namely T63 in this case, can be considered to be not completely energy consistent, which might compromise the results. For this reason an assessment of the original coupled model using the identical methods of analysis has been considered. The results for the T63 model are shown in Table A1 for the 20C period in the NPR and SPR regions. These show minor differences from the same results for the T213 20C simulation, shown in Table 1, with no identified systematic bias. Differences between the T63 and T213 simulations are believed mainly to be caused by differences of resolution and interpolation between the computational grid and the latitudes of 60°N and 60°S used for the transport calculations as well as differences caused by representation of the orography and coastal configuration. There are differences from month to month that are considered to be due to sampling and hence

Brought to you by MAX-PLANCK-INSTITUTE FOR METEOROLOGY | Unauthenticated | Downloaded 04/11/23 01:41 PM UTC

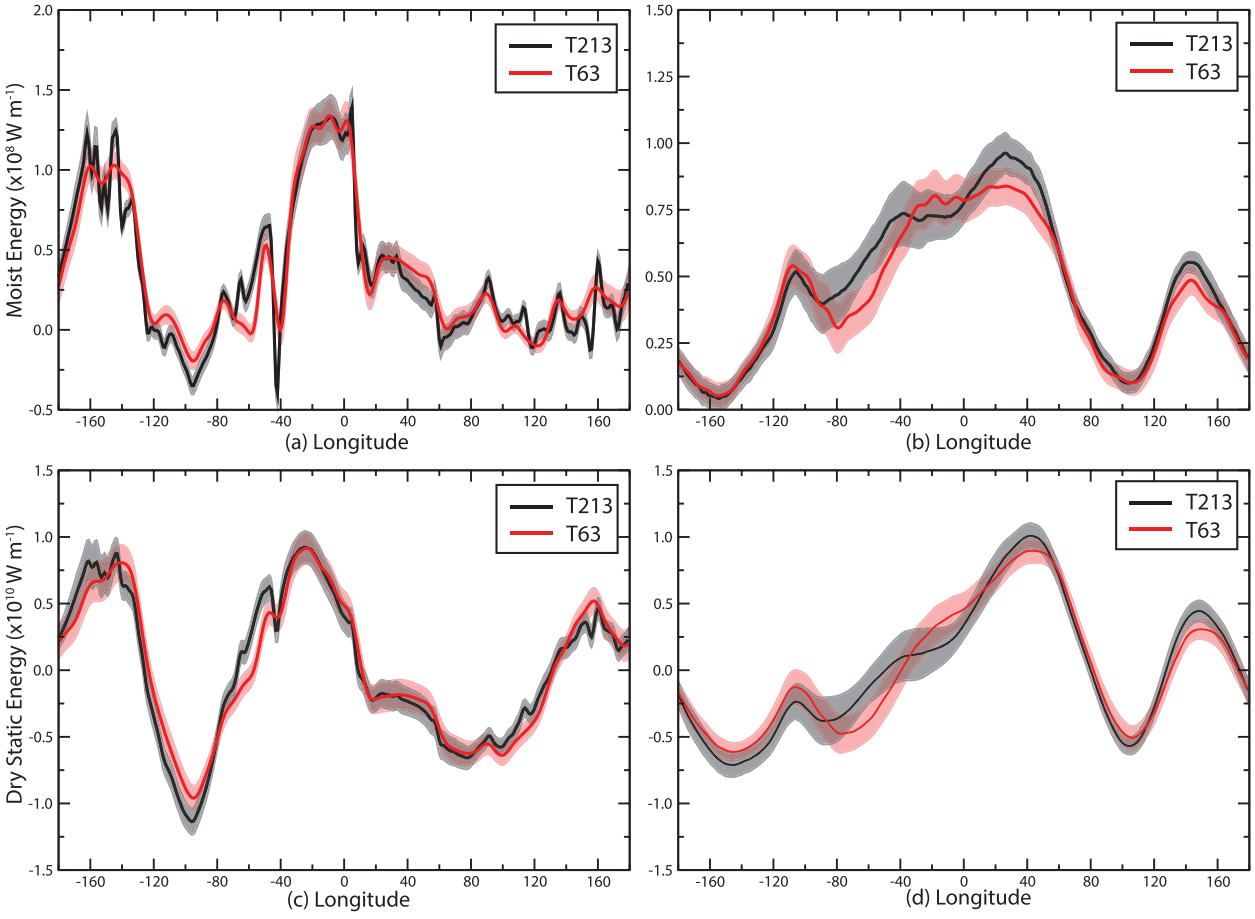

FIG. A2. Mean annual transport of energy as a function of longitude across 60°N and 60°S associated with (top) moisture and (bottom) dry static energy for T213 (black line) and T63 (red line): (a) NH moisture, (b) SH moisture, (c) NH dry static, and (d) SH dry static. Units are W m^{-1}. Shading indicates the 95% confidence intervals.

to natural variability. The residuals for both sets of simulations are of the same magnitude and on the order of 1%–2% in terms of the total net annual transport.

In Fig. A1 the annual mean vertical profiles of the total energy transport for the T63 and the T213 simulations are compared for the 20C period for the two polar regions. There are some small differences in the NPR region. Larger differences are seen for the SPR region with indications of a stronger in- and outflow for the higher-resolution model. Figure A2 shows longitudinal profiles for the moist and dry energy transports for the NPR and SPR regions for both the T63 and T213 simulations for 20C. For the moist energy transport there is considerable overlap between the two model simulations, in particular for the NPR region, but with much sharper details in the T213 simulation because the moist transport is concentrated in the lower part of the atmosphere and consequently more strongly influenced by coast lines and orography, note for example the marked differences at 40°W that is to the western side of Greenland. The dry static energy transport, which is more dominated by the transport aloft (not shown), also shows good agreement between the two simulations with considerable overlap between the two distributions, in particular for the NPR region. It is also apparent that the unit for the dry static energy is two orders of magnitude larger than the moist static energy indicating huge longitudinal compensation effects. There are somewhat larger differences between the two simulations in the SPR region for both moist and dry transports, which we believe may be due to differences in the representation of the storm tracks, the study of Bengtsson et al. (2006) showed that there were some deficiencies in the organization of the storm tracks in the SH in the T63 simulation when compared against a reanalysis and this may be resolution dependent and or dependent on differences in the large-scale stationary wave patterns but this requires further analysis to answer.

Brought to you by MAX-PLANCK-INSTITUTE FOR METEOROLOGY | Unauthenticated | Downloaded 04/11/23 01:41 PM UTC

TABLE A2. Annual mean summary of the energy budget components for 20C and 21C for T63 and T213 (parentheses). Units are W m^{-2}.

	Lq	$C_pT + gZ$	F_{WALL}	F_{SFC}	F_{RAD}	dE/dt
			NH			
20C	21.7(20.9)	68.5(64.6)	90.2(85.5)	13.4(11.5)	−102.9(−98.7)	0.7(−1.7)
21C	27.3(27.0)	65.0(58.9)	92.3(85.9)	11.5(9.1)	−103.0(−99.3)	0.8(−4.3)
21C−20C	5.6(6.1)	−3.5(−5.7)	2.1(0.4)	−1.9(−2.4)	−0.1(−0.6)	0.1(−2.6)
			SH			
20C	26.0(28.0)	61.8(56.3)	87.8(84.3)	9.7(8.0)	−95.6(−92.2)	1.9(−1.1)
21C	32.1(34.0)	53.2(47.7)	85.3(81.8)	6.1(4.2)	−92.3(−89.7)	−0.9(−3.7)
21C−20C	6.1(6.0)	−8.6(−8.6)	−2.5(−2.5)	−3.6(−3.8)	3.3(2.5)	−2.8(−2.6)

In Table A2 we finally summarize the annual mean values for 20C and 21C for both resolutions. We tentatively conclude that the T63 simulation shows a very similar behavior to the T213 simulation suggesting that the T213 simulation has not been compromised by the use of SST and sea ice boundaries taken from the T63 run; however, it would be useful to redo this analysis with a fully coupled high-resolution model.

REFERENCES

Bengtsson, L., K. I. Hodges, and E. Roeckner, 2006: Storm tracks and climate change. *J. Climate,* **19,** 3518–3543.

——, ——, and M. Esch, 2007a: Tropical cyclones in a T159 resolution global climate model: Comparison with observations and reanalyses. *Tellus,* **59A,** 396–416.

——, ——, ——, N. Keenlyside, L. Kornblueh, J.-J. Luo, and T. Yamagata, 2007b: How may tropical cyclones change in a warmer climate. *Tellus,* **59A,** 539–561.

——, ——, and N. Keenlyside, 2009: Will extratropical storms intensify in a warmer climate? *J. Climate,* **22,** 2276–2301.

——, ——, S. Koumoutsaris, M. Zahn, and N. Keenlyside, 2011a: The changing atmospheric water cycle in polar regions in a warmer climate. *Tellus,* **63A,** 907–920.

——, S. Koumoutsaris, and K. Hodges, 2011b: Large-scale surface mass balance of ice sheets from a comprehensive atmospheric model. *Surv. Geophys.,* **32,** 459–474.

Budyko, M. I., 1963: Atlas of the heat balance of the Earth sphere. Joint Geophysical Committee Presidium of the Academy of Sciences, 5 pp. and 69 plates.

Cullather, R. I., and M. G. Bosilovich, 2012: The energy budget of the polar atmosphere in MERRA. *J. Climate,* **25,** 5–24.

Fletcher, J. O., 1965: The heat budget of the arctic basin and its relation to climate. The RAND Corporation Tech. Rep. R-444-PR, 194 pp.

Haynes, J. M., C. Jakob, W. B. Rossow, G. Tselioudis, and J. Brown, 2011: Major characteristics of southern ocean cloud regimes and their effects on the energy budget. *J. Climate,* **24,** 5061–5080.

Held, I. M. and B. J. Soden, 2006: Robust responses of the hydrological cycle to global warming. *J. Climate,* **19,** 5686–5699.

Hwang, Y.-T., and D. M. W. Frierson, 2010: Increasing atmospheric poleward energy transport with global warming. *Geophys. Res. Lett.,* **37,** L24807, doi:10.1029/2010GL045440.

——, ——, and J. E. Kay, 2011: Coupling between arctic feedbacks and changes in poleward energy transport. *Geophys. Res. Lett.,* **38,** L17704, doi:10.1029/2011GL048546.

Mayer, M., and L. Haimberger, 2012: Poleward atmospheric energy transports and their variability as evaluated from ECMWF reanalysis data. *J. Climate,* **25,** 734–752.

Nakamura, N., and A. H. Oort, 1988: Atmospheric heat budgets of the polar regions. *J. Geophys. Res.,* **93** (D8), 9510–9524.

Oort, A. H., and J. P. Peixéto, 1974: The annual cycle of the energetics of the atmosphere on a planetary scale. *J. Geophys. Res.,* **79,** 2705–2719.

Porter, D. F., J. J. Cassano, M. C. Serreze, and D. N. Kindig, 2010: New estimates of the large-scale arctic atmospheric energy budget. *J. Geophys. Res.,* **115,** D08108, doi:10.1029/2009JD012653.

Reichler, T., and J. Kim, 2008: How well do coupled models simulate today's climate? *Bull. Amer. Meteor. Soc.,* **89,** 303–311.

Roeckner, E., and Coauthors, 2003: The atmospheric general circulation model ECHAM5. Part I: Model description. Max-Planck-Institut für Meteorologie Tech. Rep. 349, 127 pp.

Serreze, M. C., A. P. Barrett, A. G. Slater, M. Steele, J. Zhang, and K. E. Trenberth, 2007: The large-scale energy budget of the arctic. *J. Geophys. Res.,* **112,** D11122, doi:10.1029/2006JD008230.

Trenberth, K. E., and J. T. Fasullo, 2010: Simulation of present-day and twenty-first-century energy budgets of the southern oceans. *J. Climate,* **23,** 440–454.

——, J. M. Caron, and D. P. Stepaniak, 2001: The atmospheric energy budget and implications for surface fluxes and ocean heat transports. *Climate Dyn.,* **17,** 259–276.

Wielicki, B. A., B. R. Barkstrom, E. F. Harrison, R. B. Lee, G. L. Smith, and J. E. Cooper, 1996: Clouds and the Earth's Radiant Energy System (CERES): An Earth-observing system experiment. *Bull. Amer. Meteor. Soc.,* **77,** 853–868.

Zahn, M., and R. P. Allan, 2011: Changes in water vapor transports of the ascending branch of the tropical circulation. *J. Geophys. Res.,* **116,** D18111, doi:10.1029/2011JD016206.

——, and ——, 2013: Climate warming related strengthening of the tropical hydrological cycle. *J. Climate,* **26,** 562–574.

Zelinka, M. D., S. A. Klein, and D. L. Hartmann, 2012: Computing and partitioning cloud feedbacks using cloud property histograms. Part II: Attribution to changes in cloud amount, altitude, and optical depth. *J. Climate,* **25,** 3736–3754.

Zhang, M. H., and Coauthors, 2005: Comparing clouds and their seasonal variations in 10 atmospheric general circulation models with satellite measurements. *J. Geophys. Res.,* **110,** D15S02, doi:10.1029/2004JD005021.

Brought to you by MAX-PLANCK-INSTITUTE FOR METEOROLOGY | Unauthenticated | Downloaded 04/11/23 01:41 PM UTC